Correlation of fiber shape measures with dilute suspension properties

Emilio J. Tozzi and **Daniel J. Klingenberg**, University of Wisconsin, Madison, Wisconsin, USA, **C. Tim Scott**, USDA Forest Products Laboratory, Madison, Wisconsin, USA

KEYWORDS: Fiber shape, Shape measure, Intrinsic viscosity, Simulations

SUMMARY: The correlations between the intrinsic viscosity of fiber suspensions and 17 measures of fiber shape were investigated. The intrinsic viscosities of suspensions of fibers with various shapes and aspect ratios were determined numerically. The shapes studied include different degrees of fiber curvature, angular bends, helical shapes, randomly generated shapes, and others. The shape measure that correlated most strongly with intrinsic viscosity was an invariant of the hydrodynamic resistance tensor; this invariant is related to the hydrodynamic drag coefficients on a fiber translating in the three principal directions. This measure can be computed from 3D images of real fibers, and could potentially be a useful quantity for describing fiber shape. These results also suggest that experimentally-measured intrinsic viscosities can be used to characterize fiber shape, either directly or by extracting the invariant from experimental data.

ADDRESSES OF THE AUTHORS: Emilio J. Tozzi (ejtozzi@wisc.edu) and **Daniel J. Klingenberg** (klingen@engr.wisc.edu): University of Wisconsin, Department of Chemical and Biological Engineering and Rheology Research Center, Madison, WI 53706, USA.
C. Tim Scott (cscott@facstaff.wisc.edu): USDA Forest Products Laboratory, Madison, WI 53706, USA.
Corresponding author: Daniel J. Klingenberg

Fiber shape affects the properties of wet webs, dry sheets and pulp suspensions (Kibblewhite, Brookes 1975; Seth et al. 1983; Page et al. 1985; Switzer, Klingenberg 2003; Seth 2006). Fiber shape depends on the fibers' source, and can be altered by physical and chemical treatments (Kibblewhite, Brookes 1975; Page et al. 1985). It is thus often desirable to include measurements of fiber shape in the characterization of fiber suspensions.

Understanding the relationships between fiber shape and suspension properties is challenging, in part because fiber "shape" is difficult to quantify. Complete characterization of the geometry of an arbitrarily-shaped fiber would require an extremely large number of parameters, even when the fiber shape is idealized as a space curve. The complexity only increases when considering suspensions of fibers, in which each fiber can have a different shape, which can be altered as the suspension flows (or the web is deformed). It is therefore not surprising that efforts have focused on characterizing the average fiber shape in a suspension using a few parameters (e.g., fiber aspect ratio, curl index [Jordan, Page 1979], or kink index [Kibblewhite, Brookes 1975]). Such characterizations are necessarily incomplete (e.g., numerous fiber shapes can have the same curl index), but may correlate well with other suspension properties of interest. The challenge, then, is to select appropriate shape measures – among many possibilities – that can be measured experimentally and that correlate strongly with properties of interest.

In this report, we describe results from fiber-level simulations employed to investigate the relationship between fiber shape and suspension properties. Rigid fibers of various shapes are considered, including curved, angular, helical and randomly shaped fibers of various aspect ratios. The suspension property investigated here is the intrinsic suspension shear viscosity. Correlations between the intrinsic viscosities and numerous measures of fiber shape are determined. The curl and kink indices do not correlate strongly with the intrinsic viscosity. Several other measures of fiber shape correlate more strongly with the viscosity values. The best correlation is obtained for an invariant of the hydrodynamic friction tensor, suggesting that this parameter is a potentially more useful measure of fiber shape than the curl or kink indices (at least for describing intrinsic viscosity data). The invariant is related to the hydrodynamic drag coefficients for translation of a fiber in the three principal directions. Methods for evaluating this shape measure experimentally are suggested.

Simulation method

We consider suspensions of rigid fibers in a Newtonian fluid subjected to simple shear flow with a very small shear rate such that the Reynolds number is small. The suspensions are sufficiently dilute such that fiber interactions can be ignored [e.g., crowding number < 1 (Kerekes 2006)]. These assumptions eliminate the effects of fiber flexibility, fluid inertia and fiber interactions. Fiber motion is therefore determined entirely by hydrodynamic forces.

Each fiber is composed of several cylinders of radius r_{fiber} connected end to end. The aspect ratio is $a_r=L/(2r_{fiber})$, where L is the total length of the "backbone". We examined the behavior of suspensions of curved, angular and helical fibers (depicted in *Fig 1*) with aspect ratios 9.33, 13.75, 22.33 and 43, as well as variously shaped fibers (*Fig 2*) with aspect ratio 62.67. Prolate spheroids (not illustrated) were used as a test case for method validation.

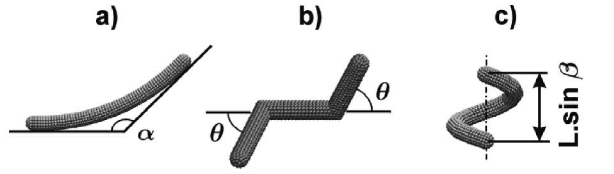

Fig 1. (a) Curved fibers have angles α ranging from 180 degrees (straight fiber) to 0 degrees (forming a "U" shape with the last segment parallel to the first one), with intermediate values at 45 degree intervals. (b) Angular fibers have angles θ of 10, 30, 50, 70 and 90 degrees. The plane formed by the first and second segments is perpendicular to the plane formed by the second and third segments. (c) Helical fibers have one turn, length L and angles β of 20, 30, 40, 50 and 60 degrees.

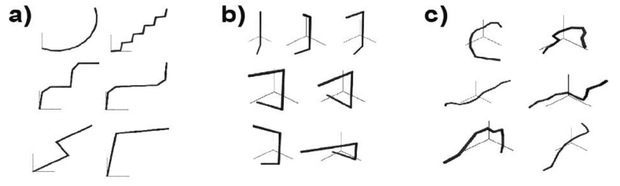

Fig 2. Fibers of aspect ratio 62.67. (a) Fibers composed of segments in the same plane. (b) Angular shapes with segments in different planes. (c) "Random" fibers composed of 10 straight segments oriented at randomly chosen angles. The angle formed by each pair of neighboring segments is restricted to lie between 180 degrees (perfectly aligned) and 135 degrees. Only 6 of the 10 random shapes used are depicted.

The motion of a rigid fiber can be described by the grand hydrodynamic resistance matrix, which relates the force, torque and stresslet on a fiber to its motion relative the ambient flow (Brenner 1964). We determined the resistance matrices for our fibers using the bead-shell method described by Carrasco and Garcia de la Torre (1999), because this technique can easily be applied for fibers of arbitrary shape.

The fiber is represented by a close-packed shell of spherical beads of radius $a << r_{fiber}$ on the fiber surface. The hydrodynamic interactions between the beads are represented using the Rotne-Prager-Yamakawa approximation (Rotne, Prager 1969; Yamakawa 1970). Solution of the forces and torques on the beads in representative flows yields the hydrodynamic resistance matrix for the fiber as a whole. This procedure produces the resistance matrix of the original (i.e., smooth) fiber in the limit $a/r_{fiber} \to 0$. However, instead of calculating the resistance matrix for successively smaller values of a/r_{fiber} and extrapolating to $a/r_{fiber} = 0$ (which requires large numbers of beads for long fibers), we found that the resistance matrices obtained for $a/r_{fiber} \approx 0.3$ with the bead centers displaced 0.5 a below the fiber surface give results of similar or better accuracy than the extrapolation method; for prolate spheroids with aspect ratios $1 \le a_r \le 50$ the resistance elements were within 3.4% of values obtained analytically (Kim, Karrilla 1991). For a prolate spheroid of aspect ratio 10 the largest error was 3.1% (the error obtained using the linear extrapolation method with $0.1 \le a/r_{fiber} \le 0.25$ and $a_r = 10$ is 4.2%).

Once the hydrodynamic resistance matrix is obtained, the fiber motion can be determined by integrating the translational and rotational velocities. Prolate spheroids in simple shear flow rotate in a closed, periodic orbit with period (Jeffery 1922)

$$\tau = \frac{2\pi}{\dot{\gamma}}\left(a_r + \frac{1}{a_r}\right), \qquad [1]$$

where $\dot{\gamma}$ is the shear rate. We compared orbit periods obtained from simulations using the "bead-shell" method described above with that predicted by *Eq 1* for $1 \le a_r \le 25$. The simulated orbit periods were within 2.2% of that predicted by *Eq 1* on average (4.5% maximum error).

To predict the intrinsic viscosity of suspensions of fibers, the motion of fibers in shear flow is simulated for different fiber shapes and different initial orientations. The fibers rotate in the shear flow in orbits that depend on the shape and initial orientation; the orbits are typically more complex than the simple Jeffrey orbits, apparently chaotic for some shapes (Yarin et al. 1997). The fiber stresslets were averaged over time and initial orientations, yielding the particle contribution to the suspension stress (Batchelor 1970). The intrinsic viscosity $[\eta]$ is defined

$$[\eta] \equiv \lim_{\phi \to 0} \frac{\eta/\eta_0 - 1}{\phi} = \lim_{\phi \to 0} \frac{\sigma^{(p)}}{\eta_0 \dot{\gamma} \phi}, \qquad [2]$$

where η is the suspension viscosity, η_0 is the suspending fluid viscosity, ϕ is the fiber volume fraction, and $\sigma^{(p)}$ is the particle contribution to the stress. To calculate the intrinsic viscosity of each shape, simulations with 300 different random initial configurations were employed, and time integrations were performed using a dimensionless time step of $\dot{\gamma}\Delta t = 5 \times 10^{-4}$ to a total dimensionless averaging time (strain) of $\dot{\gamma} t = 10^3$. To assess the validity of this approach, results for suspensions of prolate spheroids were compared with those reported by Brenner (1974). The intrinsic viscosities obtained from the simulations were within 1.6% on average of those reported by Brenner (2.3% maximum error).

Shape measures

The fiber shapes are characterized using numerous shape measures. The curl index is calculated using a definition similar to that employed by Page et al. (1985)

$$C.I. = \left(\frac{L}{e} - 1\right), \qquad [3]$$

where e is the end-to-end distance and L is the fiber contour (backbone) length.

The kink index per fiber is defined (Kibblewhite, Brooks 1975)

$$K.I. = N_{(10^\circ - 20^\circ)} + 2N_{(21^\circ - 45^\circ)} + 3N_{(46^\circ - 90^\circ)} + 4N_{(91^\circ - 180^\circ)}, \qquad [4]$$

where $N_{(\alpha-\beta)}$ is the average number of sharp bends per fiber with angles between α and β.

The hydrodynamic radius R_H (Filippov 2000) is a function of the eigenvalues of the translational friction tensor $\boldsymbol{A}$ (one component of the grand hydrodynamic resistance matrix; for translation of a fiber in a stagnant liquid, the hydrodynamic drag force $\boldsymbol{F}^H$ is related to the fiber velocity $\boldsymbol{U}$ by $\boldsymbol{F}^H = -\boldsymbol{A} \cdot \boldsymbol{U}$)

$$\frac{R_H}{L} = \left[2\pi\mu L\left(\frac{1}{\lambda_1^A} + \frac{1}{\lambda_2^A} + \frac{1}{\lambda_3^A}\right)\right]^{-1}, \qquad [5]$$

where the eigenvalues λ_1^A, λ_2^A and λ_3^A are the drag coefficients for translation of a fiber in the three principal directions (Kim, Karrila 1991).

The radius of gyration R_G is defined in terms of the centers of the beads making up the fiber surfaces (Andrews et al. 1998)

$$\frac{R_G}{L} = \frac{1}{L}\left(\frac{1}{N}\sum_{i=1}^{N} (\mathbf{r}_i - \mathbf{r}_{CM}) \cdot (\mathbf{r}_i - \mathbf{r}_{CM}) \right)^{\frac{1}{2}}, \qquad [6]$$

where $\mathbf{r}_i$ is the position of bead i, $\mathbf{r}_{CM}$ is the fiber center of mass, and N is the number of beads.

From a "form matrix" used in morphology analyses (Lele, Richtsmeier 2000), three shape measures d_1, d_2 and d_3 are defined

$$d_k = \frac{2}{N(N-1)L^k} \sum_{i=1}^{N-1} \sum_{j=1}^{N} \left| \mathbf{r}_{ij} \right|^k, \qquad [7]$$

where k = 1, 2 or 3, and $\mathbf{r}_{ij}$ is the distance between beads i and j.

The degree of prolateness DP is defined (Andrews et al. 1998)

$$DP = 27 \frac{(\lambda_1^I - \lambda_{avg.}^I)(\lambda_2^I - \lambda_{avg.}^I)(\lambda_3^I - \lambda_{avg.}^I)}{(\lambda_1^I + \lambda_2^I + \lambda_3^I)^3}, \qquad [8]$$

where λ_1^I, λ_2^I, and λ_3^I are the eigenvalues of the moment of inertia tensor I, and $\lambda_{avg.}$ is the arithmetic average of the three values. The moment of inertia tensor is

$$I = \frac{1}{N}\sum_{i=1}^{N} (\mathbf{r}_i - \mathbf{r}_{CM})(\mathbf{r}_i - \mathbf{r}_{CM}). \qquad [9]$$

Finally, the shapes are also characterized in terms of the invariants I_1, I_2 and I_3 of the various tensors described above

$$I_1 = \frac{\lambda_1 + \lambda_2 + \lambda_3}{\lambda_3}, \qquad [10]$$

$$I_2 = \frac{\lambda_1\lambda_2 + \lambda_2\lambda_3 + \lambda_1\lambda_3}{(\lambda_3)^2}, \qquad [11]$$

$$I_3 = \frac{\lambda_1\lambda_2\lambda_3}{(\lambda_3)^3}. \qquad [12]$$

The eigenvalues $\lambda_1 \square \lambda_2 \square \lambda_3$ are either those of the translational friction tensor $\boldsymbol{A}$, the rotational friction tensor $\boldsymbol{C}$ (Brenner 1964; for rotation of a fiber in a stagnant liquid, the hydrodynamic torque Γ^H is related to the fiber angular velocity Ω by $\Gamma^H = -\boldsymbol{C} \cdot \Omega$), or the moment of inertia tensor I. There are therefore nine invariants, namely I_1^A, I_2^A, I_3^A, I_1^C, I_2^C, I_3^C, I_1^I, I_2^I, and I_3^I. We show below that I_3^A is a particularly useful shape measure; as discussed above the eigenvalues λ_1^A, λ_2^A, and λ_3^A, used to calculate I_3^A via *Eq 12* are simply the hydrodynamic drag coefficients for translation of the fiber in the three principal directions (Kim, Karrila 1991).

These descriptors were selected following the criteria suggested by Beddow and Meloy (1980), that shape measures for particle characterization must be: a) rotationally invariant, b) invariant with respect to size, c) easily calculated, d) capable of relating to the mechanical behavior of the particle, and e) unequivocal and rigorous in their physical interpretation.

Results and Discussion

The intrinsic viscosities obtained from the simulations described in the Simulation Method section are plotted as a function of three shape measures in *Figs 3-5* for the variously shaped fibers of various aspect ratios described above. In *Fig 3*, the intrinsic viscosity is plotted as a function of curl index for various aspect ratios. The intrinsic viscosity tends to increase with increasing curl index, more so for large aspect ratios; for a_r = 62.67, the intrinsic viscosity varies by almost one order of magnitude as the fiber shape is varied. An increase in suspension viscosity with fiber "curvature" is consistent with experimental observations reported by Blakeney (1966), and simulations reported by Joung et al. (2002) and Switzer and Klingenberg (2003). Larger intrinsic viscosities for non-straight fibers can be explained qualitatively in terms of the dynamics of the fiber in shear flow. A non-straight fiber has a larger tumbling frequency than a straight fiber, and therefore develops larger hydrodynamic stresses, which translate into a higher intrinsic viscosity (Switzer, Klingenberg 2003).

However, the curl index is not a particularly useful measure of fiber shape, at least for characterizing the effect of shape on intrinsic viscosity. For fixed aspect ratio, the intrinsic viscosity is not a function of only the curl index; that is, in *Fig 3*, the intrinsic viscosity appears to almost collapse to a function of the curl index for each aspect ratio, but there is considerable scatter about these perceived underlying functions. This scatter occurs because the curl index does not completely capture the features of fiber shape that influence the properties of the suspension, illustrated here with the intrinsic viscosity.

The intrinsic viscosity is plotted as a function of the kink index for different aspect ratios in *Fig 4*. Although the intrinsic viscosity generally increases with kink index, there is considerably more scatter than in *Fig 3*. The kink index is also not a particularly useful measure of fiber shape for characterizing intrinsic viscosity data.

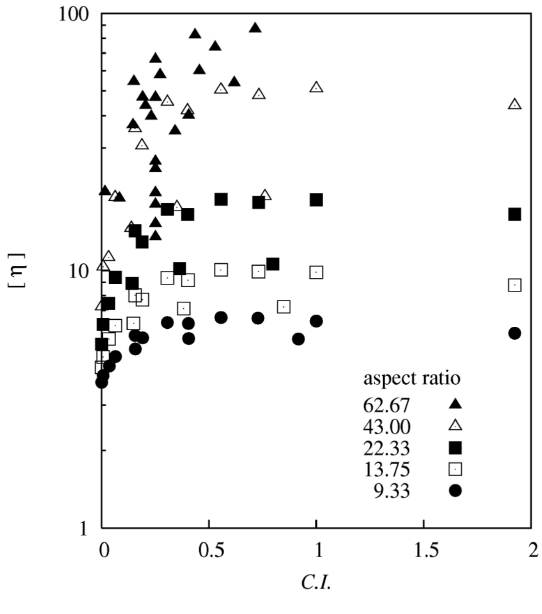

Fig 3. Intrinsic viscosity a function of curl index for various aspect ratios.

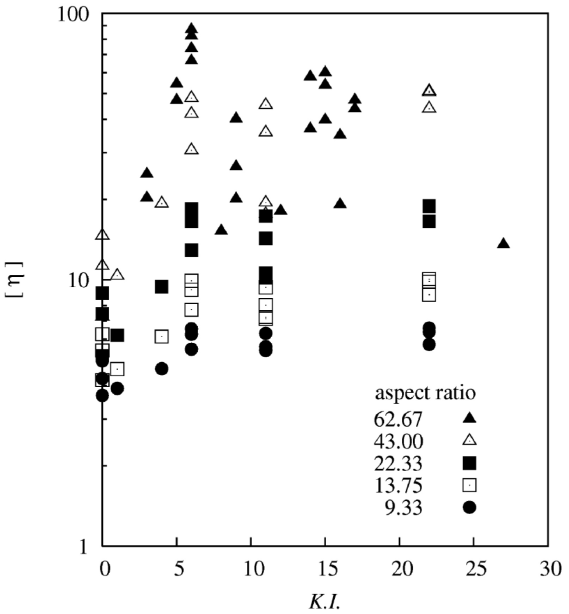

Fig 4. Intrinsic viscosity as a function of kink index for various aspect ratios.

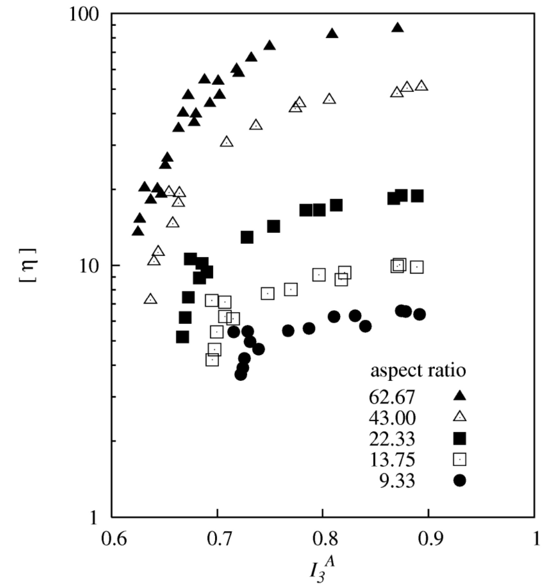

Fig 5. Intrinsic viscosity as a function of the invariant I_3^A of the hydrodynamic translational friction tensor, for various aspect ratios.

In *Fig 5*, the intrinsic viscosity is plotted as a function of the third invariant of the hydrodynamic translational friction tensor I_3^A (defined in *Eq 12*). For fixed aspect ratio, the intrinsic viscosity data collapse to a function of I_3^A, with much less scatter than observed in *Figs 3* and *4*. In this sense I_3^A is a much more useful measure for characterizing the effect of shape on fiber suspensions properties (at least for the property of intrinsic viscosity).

The intrinsic viscosity data can be reduced even further, as illustrated in *Fig 6* where the intrinsic viscosity scaled by its maximum value is plotted as a function of I_3^A for various aspect ratios. Here $[\eta]_{max}$ is the maximum value of the intrinsic viscosity obtained, which depends on the aspect ratio ($[\eta]_{max}$ is plotted as a function of the aspect ratio in the inset of *Fig 6*). All of the scaled intrinsic viscosities collapse to a single function of I_3^A. Furthermore, the scatter about the perceived master curve appears to decrease with increasing aspect ratio.

The utility of any measure for describing the effect of

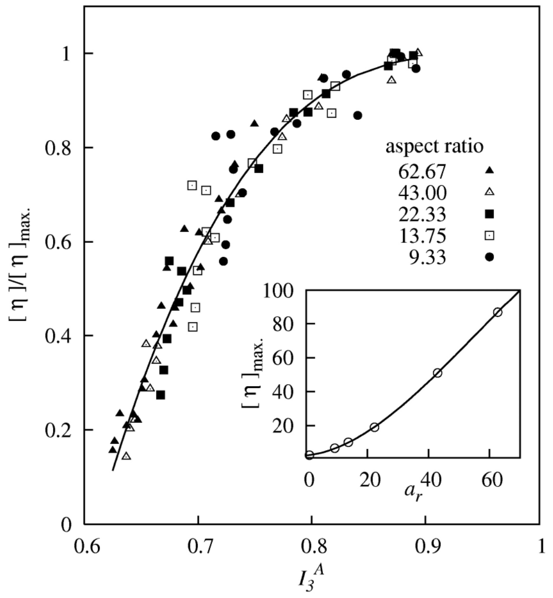

Fig 6. Scaled intrinsic viscosity $[\eta]\ /[\eta]_{max}$ as a function of the invariant of the hydrodynamic translational friction tensor I_3^A, for various aspect ratios. The inset shows the largest intrinsic viscosity [η]max as a function of the aspect ratio.

fiber shape on the intrinsic viscosity can be quantified by a coefficient that reflects the degree of correlation between the two variables. We use the standard Pearson product-moment correlation. This correlation coefficient is sensitive to outliers, a desirable feature for our purposes (Abdullah 1990). The correlation coefficients for the relationship between the intrinsic viscosity and the various shape measures described in the Shape Measures section are listed in *Table 1*. The largest correlation coefficient is obtained for I_3^A, implying that this parameter is the best for characterizing the effect of fiber shape on the intrinsic viscosity. We note that many of the shape measures correlate more strongly with the intrinsic viscosity than the curl or kink indices.

Table 1 shows that all three shape measures that utilize the eigenvalues of the hydrodynamic translational resistance tensor--- I_1^A, I_2^A, I_3^A and ---all correlate more strongly with the intrinsic viscosity than the other shape measures. It is not surprising that the intrinsic viscosity correlates strongly with the hydrodynamic drag coefficients, as these quantities are closely related. The hydrodynamic force on a particle is determined by integrating the hydrodynamic traction over the particle surface. The particle contribution to the stress from which the intrinsic viscosity is obtained is a related integral of the first moment of the hydrodynamic traction over the particle surface. It is unclear, however, why the correlation is stronger for I_3^A than for I_1^A and I_2^A.

It remains to be seen if I_3^A performs well for characterizing the shape dependence of other properties (e.g. formation, web strength, etc.). To investigate this experimentally one needs some means of determining I_3^A. In principle, one could measure the intrinsic viscosity of a suspension and then evaluate I_3^A from *Fig 5*. One can also obtain values of I_3^A by first determining the fiber shape from three dimensional images (e.g. with 3D imaging techniques such as X-Ray microtomography [Eberhardt, Clarke 2002; Lin, Miller 2005]) and then calculating I_3^A using the bead shell method described here, or any other

Table 1. Correlation coefficients between the intrinsic viscosity and various shape measures. Correlation coefficients were obtained for each aspect ratio and the absolute values were averaged. The invariants of the translational friction tensor ***A*** have the largest values.

Shape measure	Correlation coefficient	Sign
I_3^A	0.917	+
I_2^A	0.905	+
I_1^A	0.892	+
I_2^I	0.809	+
I_1^I	0.807	+
d_3	0.795	-
d_2	0.771	-
DP	0.765	+
I_3^I	0.763	+
R_G/L	0.753	-
d_1	0.735	-
I_3^C	0.692	+
I_2^C	0.664	+
I_1^C	0.623	+
C.I.	0.583	+
K.I.	0.533	+
R_H/L	0.432	-

method available to accurately predict the hydrodynamic drag on arbitrarily shaped fibers, such as slender body theory (Cox 1970) or boundary element methods (Youngren, Acrivos 1975; Allison 1999).

Finally, we note that these results illustrate that the intrinsic viscosity depends strongly on fiber shape. Experimentally-measured intrinsic viscosities can thus be used to characterize fiber shape, either directly or by extracting I_3^A from experimental data via *Fig 5*.

Conclusions

Several shape measures that account for the three dimensional geometry of fibers correlate better with the intrinsic viscosity of fiber suspensions than the curl and kink indices. This trend was observed for all fiber aspect ratios and a variety of shape classes including curved, angular, helical and random fiber shapes. An invariant of the hydrodynamic resistance tensor I_3^A (*Eq 12*), correlated most strongly with intrinsic viscosity. This invariant is related to the hydrodynamic drag coefficients on a fiber translating in the three principal directions. The invariant can easily be computed from 3D images of real fibers, and thus could represent a new valuable measure for quantifying fiber shape and its effect on suspension properties. These results also suggest that experimentally-measured intrinsic viscosities can be used to characterize fiber shape, either directly or by extracting the invariant from experimental data.

Acknowledgments

The project was supported in part by the National Research Initiative of the USDA Cooperative State Research, Education and Extension Service, grant number 2006-35504-17401.

Literature

Abdullah, M.B. (1990): On a robust correlation-coefficient, Statistician, 39 (4): 455-460.

Allison, S.A. (1999): Low Reynolds number transport properties of axisymmetric particles employing stick and slip boundary conditions, Macromolecules, 32, 5304-5312.

Andrews, N.C., Mc Hugh, A.J. and Schieber, J.D. (1998): Conformational and rheological dynamics of semiflexible macromolecules undergoing shear flow: A nonequilibrium Brownian dynamics study, J. Rheol. 42 (2):281-305.

Batchelor, G.K. (1970): The stress system in a suspension of force-free particles, J. Fluid Mech. 41, 545-570.

Beddow, J.K. and Meloy, T. (1980): Testing and Characterization of Powders and Fine Particles, Heyden, London.

Blakeney, W.R. (1966): The viscosity of suspensions of straight, rigid rods, J. Colloid Interface Sci. 22, 324-330.

Brenner, H. (1964): The Stokes resistance of an arbitrary particle-II. An extension, Chem. Eng. Sci. 19, 599-629.

Brenner, H. (1974): Rheology of a dilute suspension of axisymmetric Brownian particles, Int. J. Multiphase Flow, 1, 195-341.

Carrasco, B. and Garcia de la Torre, J. (1999): Hydrodynamic Properties of Rigid Particles: Comparison of Different Modeling and Computational Procedures, Biophys. J. 76, 3044-3057.

Cox, R.G. (1970): The motion of long slender bodies in a viscous fluid. Part 1. General Theory, J. Fluid Mech. 44, 791-810.

Eberhardt, C.N. and Clarke, A.R. (2002): Automated reconstruction of curvilinear fibres from 3D datasets acquired by X-ray microtomography, J. Microsc. 206, 41-53.

Filippov, A.V. (2000): Drag and Torque on Clusters of N Arbitrary Spheres at Low Reynolds Numbers, J. Colloid Interface Sci. 229, 184-195.

Jeffery, G.B. (1922): The Motion of Ellipsoidal Particles Immersed in a Viscous Fluid, Proc. Royal Soc. Lond. A 120, 161-179.

Jordan, BD. and Page, D.H. (1979): Application of image analysis to pulp fiber characterization. In: Proceedings of the International Paper Physics Conference, Harrison Hot Springs, BC. CPPA, Montreal, pp. 105-114.

Joung, C.G., Phan-Tien, N. and Fan, X.J. (2002): Viscosity of curved fibers in suspension, J. Non-Newtonian Fluid Mech. 102, 1-17.

Kerekes, R.J. (2006): Rheology of fibre suspensions in papermaking: An overview of recent research, Nord. Pulp Paper Res. J. 21(5), 598-612.

Kibblewhite, R.P. and Brookes, D.B. (1975): Factors which influence the wet web strength of commercial pulps, Appita, 8(4), 227-231.

Kim, S. and Karrila, S.J. (1991): "Microhydrodynamics", Butterworth-Heinemann, London.

Lele, S. and Richtsmeier J.T. (2000): Statistical Models for Landmark Coordinate Data, In: "An invariant approach to statistical analysis of shapes", Chapman and Hall/CRC Press, Interdisciplinary Statistics series. London.

Lin, C.L. and Miller, J.D. (2005): 3D characterization and analysis of particle shape using X-ray microtomography (XMT), Powder Technol. 154, 61-69.

Page, D.H., Seth, R.S., Jordan, B.D. and Barbe, M.C. (1985): Curl, crimps, kinks and microcompressions in pulp fibres: Their origin, measurement and significance. Proc. 8th Fund. Res. Symp.: Fundamentals of papermaking, Oxford UK, Volume 1, pp. 183-227. Mech Eng. Publ. London.

Rotne, J., and Prager, S. (1969): Variational Treatment of Hydrodynamic Interaction in Polymers, J. Chem. Phys. 50, (11):4831-4837.

Seth, R.S., Page, D.H., Barbe, M.C. and Jordan, B.D. (1983): The mechanism of the strength and extensibility of wet webs, Proceedings of the 1983 International Paper Physics Conference, Harwich Port, MA, pp. 73-80.

Seth, R.S. (2006): The importance of fibre straightness for pulp strength, Pulp Paper Can. 107 (1): 34-42.

Switzer, L. and Klingenberg, D. J. (2003): Rheology of sheared flexible fiber suspensions via fiber-level simulations, J. Rheol. 47 (3), 759-778.

Yamakawa, H. (1970): Transport Properties of Polymer Chains in Dilute Solution: Hydrodynamic Interaction, J. Chem. Phys. 53, (1):436-443.

Yarin, A.L., Gottlieb, O. and Roisman, I.V. (1997): Chaotic rotation of triaxial ellipsoids in simple shear flow, J. Fluid Mech. 340, 83–100.

Youngren, G. and Acrivos, A. (1975) Stokes flow past a particle of arbitrary shape: a numerical method of solution, J. Fluid Mech. 69, 377-403.

Manuscript received January 18, 2008
Accepted August 20, 2008